ELSEVIER

Chemical Geology 220 (2005) 47–66

CHEMICAL GEOLOGY
INCLUDING
ISOTOPE GEOSCIENCE

www.elsevier.com/locate/chemgeo

Zircon U–Pb chemical abrasion ("CA-TIMS") method: Combined annealing and multi-step partial dissolution analysis for improved precision and accuracy of zircon ages

James M. Mattinson

Department of Geological Sciences, University of California, Santa Barbara, CA 93106, USA

Received 2 August 2004; received in revised form 18 January 2005; accepted 2 March 2005

Abstract

A long-standing goal in high-precision and high-accuracy U–Pb zircon geochronology is the total elimination of discordance caused by Pb loss. In theory, this is fairly straightforward, but in reality it has proven extremely difficult to attain (or even demonstrate attainment of) this goal. However, a new method, "CA (Chemical Abrasion)-TIMS", is capable of completely removing zircon domains that have lost Pb, and then analyzing residual, perfectly closed-system zircon. CA-TIMS uses high-temperature treatment (in the range of 800–1100 °C for 48 h) to anneal zircon lattice radiation damage from natural alpha, alpha recoil, and spontaneous fission processes; this annealing eliminates elemental and isotopic leaching effects that have limited earlier efforts at chemical "leaching" or multi-step "step-wise dissolution" or "partial dissolution analysis (PDA)". The annealed zircons are then subjected to a series of partial dissolution steps at progressively higher temperatures. These steps initially remove (usually outer) zircon zones with high U+Th concentrations. These earliest partial dissolution steps are invariably slightly to strongly discordant, due to Pb loss. Later steps sample progressively lower U+Th zircon domains. In zircon samples that lack inheritance, these later steps sample zircon domains that are completely free from Pb loss, defining $^{206}Pb^*/^{238}U$ plateau ages with precisions (and accuracies, subject to decay constant and tracer calibration accuracies) better than 0.1%.

Keywords: Geochronology; Zircon; U–Pb; Annealing; Chemical abrasion

1. Introduction

Since the inception of U–Pb isotopic dating of zircons (Tilton et al., 1955), partially open system behavior (Pb loss) has been recognized as a major factor limiting the accuracy of zircon age determinations. Over the years, various methods have been developed to deal with Pb loss. These range from the famous graphical concordia diagram (Wetherill, 1956), to various chemical and physical "pre-treatments" and grain selection techniques aimed at reducing the degree of discordance. As detailed below, chemical ("strong" acid washing, "leaching", and partial dissolution), as well as mechanical (air

E-mail address: mattinson@geol.ucsb.edu.

0009-2541/$ - see front matter © 2005 Elsevier B.V. All rights reserved.
doi:10.1016/j.chemgeo.2005.03.011

abrasion) methods have been applied with varying degrees of success. This paper describes a new zircon analysis method that combines high-temperature annealing of pre-existing radiation damage, with multi-step partial dissolution analysis (PDA). It demonstrates for a variety of zircon samples that this new "chemical abrasion", or "CA-TIMS" method can completely remove those domains of zircon grains that have lost Pb, and thus yield highly precise and accurate ages for zircon crystallization.

For many years, methods using chemical leaching or partial dissolution of zircon to remove radiation-damaged domains associated with Pb loss have shown considerable promise for more accurate and precise U–Pb dating, but have fallen short of fulfilling this promise. A few early studies extend back to the earliest applications of U–Pb isotopic dating in the 1950s and 1960s. For example, Tilton (1956) investigated "the interpretations of lead–age discrepancies by acid washing experiments", and Silver and Deutsch (1963) experimented with "stripping" zircons by partial dissolution using the borax fusion method (then the standard method for digesting zircons). A major revolution in zircon geochronology, the development of methods of digesting zircon with HF in Teflon capsules at high temperatures and pressures (Krogh, 1973), led to a great increase in the number of laboratories around the world performing zircon geochronology. Krogh and Davis (1974, 1975) followed that breakthrough in analytical methods by demonstrating that discordant zircons commonly contain altered domains that can be strongly etched by HF vapor, that HF leaching can remove these altered domains, and that much of the Pb loss is associated with these domains; such leaching leaves a residue much more concordant than the original bulk zircon. Todt and Büsch (1981) took an important next step in partial dissolution analysis by analyzing zircons in as many as seven sequential steps, with full isotopic analysis of each step. However, the results were complex, with a strong variation in isotopic systematics from step to step, including alternately strongly reversely discordant ($^{206}Pb^*/^{238}U$ age $\gg$ $^{207}Pb^*/^{206}Pb^*$ age) and normally discordant steps. This suggested serious problems with the specific analytical techniques used.

The rather discouraging multi-step dissolution results of Todt and Büsch (1981) were shortly followed by yet another breakthrough by Krogh (1982) who demonstrated that major improvements in concordance could be achieved by removing the outer zones of zircon grains via air abrasion. The simple mechanical removal of the outer (usually higher U+Th) zircon zones was effective and simple to understand. As a result, air abrasion was almost universally accepted and applied as a routine treatment for zircons prior to dissolution for isotopic analysis; few workers continued to pursue leaching or partial dissolution studies. However, Mattinson (1994) was able to show that most of the enigmatic isotopic systematics reported for multi-step zircon dissolutions by Todt and Büsch (1981) were related to the specific dissolution and spiking methods used in that study. These results were promising, and this and subsequent studies suggested that detailed multi-step partial dissolution analysis (PDA) was useful in zircons with Pb loss, with Pb loss plus inheritance, and even with reverse discordance (e.g. Mattinson, 1994; McClelland and Mattinson, 1996; Mattinson et al., 1996).

Subsequent studies, especially on zircons with high levels of radiation damage, revealed previously unrecognized complexities in some PDA analyses, with early partial dissolution steps leaching Pb* from the remaining, undigested zircon. Effects of this leaching included not only fractionation of U/Pb* ratios, but also of $^{207}Pb^*/^{206}Pb^*$ ratios. These effects were first described by Mattinson (1997), who noted:

Some zircon samples show much more complex behavior for the early stages of dissolution. In these cases, an initial step, even with dilute acids and at relatively low temperatures, may contain not only the U and Pb associated with the small volume of zircon actually dissolved, but also excess Pb* and ^{234}U leached from the residual zircon. Pb*, ^{234}U, and other intermediate daughter products occupy alpha-recoil-damaged sites, and have been displaced by alpha recoil to surfaces, microcracks, fission tracks, etc., that provide access to corrosive solutions either in the laboratory or in nature. Significant isotopic fractionation (preferential leaching of $^{206}Pb^*$ relative to $^{207}Pb^*$) is also observed, presumably related to the difference in overall decay energy released in the production of $^{206}Pb^*$ versus $^{207}Pb^*$. Subsequent partial dissolution steps are thus depleted in Pb*, ^{234}U, and $^{206}Pb^*$, but show progressive 'recovery' such that the final steps and residues show no leaching or fractionation effects.

Later, similar effects were reported by Davis and Krogh (2000), Corfu (2000), and Chen et al. (2002). However, especially in the Davis and Krogh (2000) and Corfu (2000) studies of Archean zircons, the very small final residues still showed significant leaching effects. There is general agreement about the elemental (U vs. Pb) leaching effects. They are related to the fact that all radiogenic isotopes in the U–Pb (and Th–Pb) decay chains reside in alpha-recoil-damaged sites. This is in contrast to the lattice-bound parent isotopes of U and Th. Thus Pb* and any of the intermediate daughter products are more readily leached from zircons than their long-lived parent isotopes.

The isotopic fractionation of ^{207}Pb* and ^{206}Pb* is more controversial however. Two end-member models are as follows. Mattinson (1997, 2000a) suggested that the difference in the number of alpha decays and in the energies of those decays slightly but significantly favors the leaching of ^{206}Pb* over ^{207}Pb*. In this model, the ca. 6–8% greater aggregate length of the ^{206}Pb* alpha-recoil tracks (e.g., Mattinson, 2000a; Nasdala et al., 2001, 2002) results in a greater probability of a fission track, for example, intersecting an alpha-recoil track of ^{206}Pb* rather than an alpha-recoil track of ^{207}Pb*. If a network of intersecting microcracks, fission tracks, and alpha-recoil tracks provides access for corrosive fluids, ^{206}Pb* will be leached preferentially, compared to ^{207}Pb*. This explains the artificially low ^{207}Pb*/^{206}Pb* age of the first PDA step, and the artificially high ^{207}Pb*/^{206}Pb* ages of subsequent step(s) that have been depleted in ^{206}Pb* by the earlier step(s). Romer (2003) has also discussed the importance of alpha-recoil track lengths in the U–Pb system. Davis and Krogh (2000) suggested a contrasting model in which the differences in alpha-recoil track lengths play no role. Instead, they suggested that the isotopic fractionation results from a thermal event during the geologic past. In this model, "old" (high ^{207}Pb*^{206}Pb*) Pb produced between the time of original zircon crystallization and the thermal event (of sufficient temperature and duration to anneal the alpha-recoil lattice damage) is sequestered in the annealed lattice, and is immune to leaching. "Young" (lower ^{207}Pb*/^{206}Pb*) Pb produced after the thermal event resides in still-damaged sites and is readily leached. According to this model, the "too-young" ^{207}Pb*^{206}Pb* age for the first PDA step results because this step preferentially does extract "young" radiogenic Pb, generated during the post-annealing part of the zircon's lifetime. The "too-old" ^{207}Pb*^{206}Pb* ages for later PDA steps are explained because these steps preferentially extract the older Pb* generated during the pre-annealing part of the zircon's lifetime. These different models will be discussed in more detail elsewhere.

Mattinson (2000b, 2003) also noted that pre-digestion laboratory annealing of radiation damage greatly suppressed the U–Pb and Pb/Pb fractionation effects discussed above. A series of detailed experiments into annealing temperatures and dissolution techniques (e.g., Mattinson, 2000b) revealed that annealing at increasingly higher temperatures progressively reduces zircon solubility as well as the leaching/fractionation-related isotopic complexities. Over a broad range of annealing temperatures (ca. 800–1100 °C for 48 h), radiation damage and related leaching effects are completely eliminated for zircon domains with low to moderate original radiation damage. Equally important, the annealing does not introduce any detectable disturbance in the U–Pb isotopic system. This is consistent with experiments showing very high closure temperatures for Pb in crystalline zircon (Lee et al., 1997; Cherniak and Watson, 2000). The resulting "CA (chemical abrasion)-TIMS" method of zircon analysis, combining pre-analysis high-temperature annealing followed by multi-step PDA, is remarkably effective at complete removal of zircon domains that have been affected with Pb loss, and is the focus of this study. In the absence of inheritance, the CA-TIMS technique can generate high-precision, high-accuracy multi-step plateau ages (analogous to ^{40}Ar/^{39}Ar plateau ages) at better than 0.1% accuracy levels (excluding decay constant and tracer calibration uncertainties). More complex isotopic systematics (e.g., inheritance of zircons with a range of ages) are easily recognized, but not always easily interpreted for multi-grain zircon fractions. In these cases, application of the CA-TIMS technique to single zircon grains completely removes the effects of Pb loss, allowing more accurate identification of grains with inheritance versus those completely lacking inheritance (e.g., Mundil et al., 2004).

2. Analytical methods

Zircon samples were prepared by the usual mineral separation and purification methods. For the present study, zircon samples demonstrated by previous work to lack inheritance were used. Very large samples (in the range of a few milligrams to tens of milligrams) allowed ca. 10–15 steps for each sample, high-precision analyses even of steps containing <1% of the total Pb and U in the sample, and static collection with Faraday cups on the major Pb isotopes for the best accuracy and precision on $^{207}Pb^*/^{206}Pb^*$ ages. Based on experience from earlier work (Mattinson, 2000b), the samples were annealed in high-purity alumina crucibles in air, except for un-annealed control samples. Samples in this study analyzed by the full CA-TIMS method were annealed at 850 °C or 1100 °C for 48 h. All samples were then subjected to a series of partial dissolution analysis (PDA) steps. Typically, for each step, the samples in 3 ml screw-top PFA Savillex vials, were spiked with a mixed $^{205}Pb/^{235}U$ tracer, and partially digested in a mixture of 10 parts 50% HF plus 1 part 8 M HNO3 in PARR digestion vessels. For some studies, the first PDA step used only 5% HF. Early PDA steps used relatively low temperatures (e.g., 80 to 140 °C) for 12–24 h. Subsequent steps used progressively higher temperatures (e.g., 150 to 200 °C), also for 12–24 h. In some cases, the sample was exhausted by repeated steps at the high end of the temperature range. In other cases, based on visual inspection indicating that only a very small residue remained, the series of PDA steps was halted, and the remaining zircon residue was totally digested at 240 °C for ca. 72 h. In all cases the 3 ml sample vials were stacked three-deep in the 45 ml PARR digestion vessels. About 1.5 ml of HF+HNO_3 mixture, identical to the mixture inside the 3 ml vials, was added to the PARR Teflon cup to ensure equivalent vapor pressure inside and outside the sample vials. This allowed the sample vial caps to be tightened "firm-finger-tight", so that the vials are ca. closed systems.

After each HF partial digestion step, the samples were completely evaporated to dryness. The samples were then subjected to a thorough HCl pick-up/clean-up procedure that has a series of crucial but different goals. First, it is essential that the U and Pb from each step accurately represent the volume of digested zircon, and is completely equilibrated with the U+Pb tracer. Pre-spiking, use of adequate HNO_3 to maintain strongly oxidizing conditions (Krogh, 1973), evaporation to dryness, and a thorough pick-up step in HCl all contribute to achieving this goal. Second, all remnants of sample and spike U and Pb must be removed prior to the next step, both from the zircons themselves, and from the walls of the Teflon digestion vials. This was achieved by additional "clean-up steps". No doubt a variety of pick-up/clean-up procedures would be adequate, and in fact a range of methods was experimented with during the course of the study. The most recent procedure is as follows: after evaporation of the HF to dryness on a hot plate, ultra-pure 3.1 N HCl is added (in an amount appropriate for the sample size and column chemistry as in a normal single-step zircon analysis) for the sample pick-up step. The vials, again capped "finger tight", are placed back in the PARR vessels (with 1.5 ml 3.1 N HCl in the PARR Teflon cup to maintain equal vapor pressure inside and outside the sample vials), and returned to the oven for 12 h at 160 °C. After cooling, the sample solution is pipetted out of the Teflon vial into a small centrifuge tube, taking care not to pipette out any zircon grains. The sample solution is centrifuged, and is then ready for column chemistry. The zircon residue is rinsed several times with ultra-pure H_2O, which is carefully pipetted off and discarded. A few drops of 8 N HNO_3 is added to the zircon residue, and the residue is transferred, by pouring, into a second, freshly cleaned PFA vial. The HNO_3 and several H_2O rinses are pipetted off and discarded. Two milliliters of fresh HCl is then added (obviously this is scaled down for small samples in micro-capsules). The samples in the PARR vessels are returned to the oven for 20 h at 160 °C. After cooling, this solution is pipetted off and discarded. Again, the residue is rinsed several times in ultra-pure H_2O, and finally in ultra-pure 8 N HNO_3. At this stage, the sample in a small remaining drop of HNO_3 is spiked, fresh HF and HNO_3 added, and placed in an oven for the next PDA step. Meanwhile, the first sample vial is subjected to normal high-temperature cleanup steps, and set aside for the following PDA step.

Pb and U were purified using the HCl ion exchange chemistry described by Krogh (1973). Columns with a resin bed volume of 0.15 ml were used, because some PDA steps dissolved up to a few mg of zircon. Pb blanks were typically in the range of 4–8

pg. For the first one or two PDA steps, some large samples contained significant impurities. For these steps, the Pb and U were stripped separately using 6 N HCl and H_2O, respectively. For these early steps, Pb was loaded separately on filaments for mass spectrometry using silica gel. U was further purified using UTEVA resin, then loaded using silica gel on the previously used Pb filaments from the respective Pb runs, and run as UO_2. For all the subsequent steps, the Pb and U were stripped simultaneously using H_2O, and were loaded together using silica gel. Pb was run first, then UO_2.

Zr was recovered from the ion exchange column washings, and concentrations were determined by ICP-AES. This permitted assessment of the actual amount of zircon digested in each step, and calculation of the U concentration of the zircon digested in each step. As discussed later, this information is quite useful for understanding both Pb loss related to natural radiation damage, and also the partial dissolution behavior of the zircon sample. In some cases, an aliquot of this solution was reserved for further trace element analysis (e.g., REE by ICP-MS).

Both Pb and U were run on the UCSB Finnigan-MAT-261 multicollector instrument in the static multicollection mode. All the major Pb isotopes were collected on Faraday cups. With the exception of some of the early steps, the ^{204}Pb signal was very small and was collected simultaneously by ion counting on a Spectromat ion counting system. In most cases, later PDA steps contained virtually zero initial Pb. Mass fractionation and any minor Faraday collector biases were corrected relative to the NBS-982 equal-atom Pb standard. The ion counter was calibrated by comparing the Faraday/Faraday versus Faraday/ion counting $^{206}Pb/^{204}Pb$ ratios for the NBS-983 radiogenic Pb standard.

3. Results and discussion

3.1. Experimental rationale

The following discussion focuses predominantly on multi-step $^{206}Pb^*/^{238}U$ age release spectra for zircon samples. $^{206}Pb^*/^{238}U$ ages provide the most rigorous test of the new method because they can be measured with high precision and are the most sensitive to any analytical fractionation effects. They also have the potential to provide the most precise and accurate ages, especially on small samples and young samples, again for reasons of analytical precision and accuracy, and lack of error magnification from decay constant uncertainties. $^{207}Pb^*/^{206}Pb^*$ ages can produce excellent plateau results, as discussed later, but especially for Paleozoic and younger samples, are subject to much larger possible random and systematic errors related to measurement uncertainties, common Pb corrections, intermediate daughter product (IDP) disequilibrium effects, and decay constant error magnification (e.g., Mattinson, 1987; Ludwig, 2000a). Within these limitations, agreement or disagreement of $^{207}Pb^*/^{206}Pb^*$ ages with $^{206}Pb^*/^{238}U$ ages is still a primary indicator of concordance or discordance. However, for zircons that lack inheritance, the possible uncertainties in calculated $^{207}Pb^*/^{206}Pb^*$ ages further emphasize the importance and robustness of the $^{206}Pb^*/^{238}U$ decay system, and of the multi-step plateau method for ages of the highest accuracy.

First, two un-annealed samples are discussed, illustrating the range of open system (leaching) to ca. closed system behavior from early to late PDA steps. Next, three aliquots of zircon, un-annealed, weakly annealed, and more strongly annealed, respectively, reveal the progressive suppression of solubility and leaching effects by the annealing of radiation damage. Finally, a series of samples analyzed by the complete CA-TIMS method demonstrate the precision and accuracy of the new approach to U–Pb zircon dating.

3.2. Un-annealed samples

Results for sample 1, zircons from an Early Cretaceous pluton from Baja California (Busby et al., in press) are shown in Fig. 1 and Table 1. A large zircon fraction, un-annealed, was analyzed in 14 PDA steps. The age versus U released pattern (Fig. 1A) is typical of the behavior first discussed by Mattinson (1997). This diagram is analogous to the well-known $^{40}Ar/^{39}Ar$ release spectrum, following Mattinson (1994) in its application to the U–Pb system. The initial (A) step is a very low-intensity step using 10 parts 5% HF/1 part 8 N HNO_3, 24 h at 80 °C in an oven. Nevertheless, it removed 8.8% of the total U in

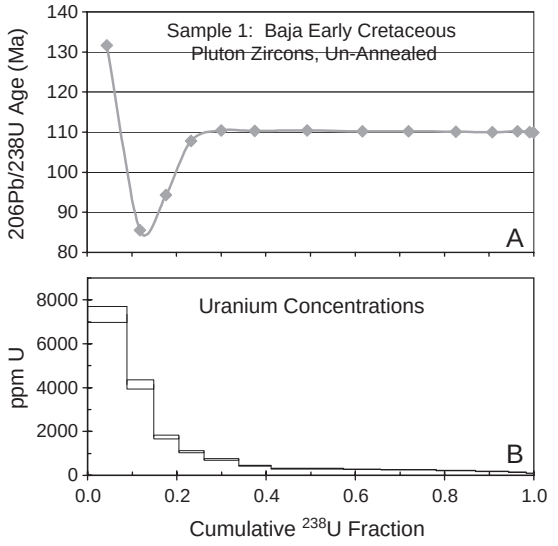

Fig. 1. Multi-step PDA results for sample 1 un-annealed Early Cretaceous zircons. The initial PDA step ("A" in Table 1) plots at the left side of the diagram; the higher temperature PDA steps plot progressively towards the right side (analogous to a $^{40}Ar/^{39}Ar$ step heating release diagram). (A) $^{206}Pb^*/^{238}U$ age release pattern showing strong leaching effects for the first four PDA steps, and good age agreement for the remaining 10 PDA steps (see text for more detailed discussion). Data points are fitted with a simple spline curve for visualization of the leaching effects in the early steps. (B) U concentration data for each step. Width of each box represents the fraction of the total U released for each step. Height of each box represents a 5% uncertainty in the U concentration (mostly from ICP-AES uncertainties).

the zircon sample. As shown in Fig. 1B, the zircon digested in the A step is high in U (ca. 7300 ppm), and thus readily soluble due to high levels of accumulated radiation damage. Moreover, in addition to removing the Pb associated with the zircon actually digested, the A step also evidently leached additional radiogenic Pb from layers deeper within the zircon. Presumably the A step etched fission tracks, microcracks, etc., in the residual zircon and used them as fluid conduits to access and leach radiogenic isotopes from their alpha-recoil-damaged sites (e.g., Mattinson, 1997, 2000a). Thus, the A step yields a $^{206}Pb^*/^{238}U$ age that is about 20% older than the actual crystallization age of the sample. Not surprisingly, the following B step (10 parts 50% HF/1 part 8 N HNO_3, 24 h at 80 °C) reflects a strong depletion in radiogenic Pb, yielding a low apparent $^{206}Pb^*/^{238}U$ age. This step, despite the use of full strength HF, removed only 6% of the total sample U, reflecting a significantly lower (but still fairly high) U concentration of ca. 4100 ppm. The overall isotopic mass balance of the B step evidently reflects three components: 1) the U and Pb in the actual volume of zircon fully digested in the B step; 2) minus the Pb leached by the A step; 3) plus any Pb leached by the B step from the remaining zircon. The next two (C and D) steps show progressive recovery from the depletion (see Table 1 for details of digestion conditions) and progressively lower U, at ca. 1500 and 1100 ppm, respectively. The isotopic mass balance of the C step is likely similar to that of the B step. However, the D step evidently was unable to leach a significant amount of Pb from the zircon residue remaining after that step, as indicated by the fact that the remaining 10 steps yield ages in good agreement with each other. Presumably the levels of natural radiation damage in the inner parts of the zircon were low enough that there was insufficient communication between fission tracks, alpha recoil tracks, etc., for there to be any further major leaching effects. Together, the first four steps represent about 26% of the total U in the sample. These first four steps, recombined, yield a $^{206}Pb^*/^{238}U$ age of 107.8 Ma. This is significantly lower than the average age of the higher T steps (discussed next), evidently reflecting the small degree of natural Pb loss experienced by these zircons.

The remaining 10 PDA steps, representing about 74% of the U in the zircons, show a further strong decrease in U concentrations (Fig. 1B), from ca. 730 ppm (E) to ca. 70 ppm (N). I interpret the U concentration data as very strong evidence that the PDA steps first attacked late-crystallized, high-U rim material (and possibly high-U interior zones, see Mattinson, 1994). The later, higher intensity PDA steps progressively digested earlier crystallized, lower-U domains from the deep interiors of the grains. The E through N steps have approximately equal $^{206}Pb^*/^{238}U$ ages, yielding an average age of 110.16 ± 0.12 Ma (2-sigma error; $\pm 0.2\%$ errors on individual points; MSWD = 2.2) using Ken Ludwig's Isoplot program (Ludwig, 2000b). In detail however, the ages appear to show a slight decline in age from ca. 110.4 to ca 109.9 Ma from the E through N steps. This apparent decline, plus the slightly high MSWD might simply be statistical variation, but alternatively

Table 1
U–Pb data for zircons

Sample	Anneal	Weight (mg)	PDA conditions	% of total U	U (ppm)	Observed ratio	Calculated ages (Ma)			Calculated ratio
						$^{206}Pb/^{204}Pb$	$^{206}Pb^*/^{238}U$	$^{207}Pb^*/^{206}Pb^*$	Error (2-sigma)	$^{232}Th/^{238}U$
Sample 1										
A step	None	0.27	5%/80 °C/24 h	8.82	7336	259	131.60	97.3	43.0	0.336
B step		0.32	50%/80 °C/24 h	5.98	4146	374	85.50	147.3	28.0	0.188
C step		0.73	50%/100 °C/24 h	5.70	1752	1819	94.30	148.3	8.0	0.151
D step		1.16	50%/120 °C/24 h	5.58	1082	3451	107.80	135.3	4.0	0.152
E step		2.41	50%/140 °C/24 h	7.82	729	5546	110.36	120.7	2.5	0.196
F step		3.72	50%/150 °C/24 h	7.19	434	7258	110.32	113.6	2.0	0.414
G step		3.25	50%/160 °C/24 h	16.32	308	16,926	110.40	112.9	1.2	0.614
H step		5.41	50%/160 °C/24 h	8.35	277	23,588	110.19	112.1	1.1	0.649
I step		11.01	50%/170 °C/24 h	12.37	252	42,040	110.19	112.1	0.9	0.637
J step		9.14	50%/170 °C/24 h	8.82	217	65,538	110.08	112.7	0.8	0.608
K step		9.29	50%/180 °C/24 h	7.43	180	72,784	110.03	112.7	0.8	0.580
L step		6.31	50%/190 °C/24 h	3.96	141	37,167	110.16	114.1	0.9	0.537
M step		3.32	50%/190 °C/24 h	1.46	99	19,991	109.96	113.0	1.2	0.487
N step		0.59	Residue digest	0.19	71	7403	109.93	122.3	10.0	0.436
Sample 2										
A step	None	0.39	5%/80 °C/24 h	18.03	11,743	2868	101.30	73.7	5.0	0.783
B step		0.59	50%/80 °C/24 h	11.00	4777	11,636	63.56	113.3	1.4	0.656
C step		0.91	50%/100 °C/24 h	8.62	2427	21,564	77.26	107.7	1.0	0.627
D step		1.36	50%/120 °C/24 h	8.55	1603	28,837	86.00	95.3	0.9	0.610
E step		3.01	50%/140 °C/24 h	13.61	1155	55,748	86.70	91.1	0.9	0.602
F step		5.18	50%/150 °C/24 h	16.62	819	83,540	86.88	89.4	0.8	0.568
G step		3.63	50%/160 °C/24 h	8.63	608	90,754	86.73	90.1	0.8	0.541
H step		4.49	50%/160 °C/24 h	8.61	490	64,848	86.85	89.2	0.8	0.521
I step		3.67	50%/170 °C/24 h	5.53	385	47,373	87.10	91.0	0.9	0.499
J step		0.71	50%/170 °C/24 h	0.79	287	31,048	87.33	90.5	2.2	0.510
Sample 3										
A step	None	na	5%/80 °C/24 h	18.82	na	1123	116.96	92.5	5.0	0.105
B step		na	50%/80 °C/24 h	11.97	na	8315	72.63	150	2.0	0.095
C step		na	50%/120 °C/24 h	7.12	na	5161	80.11	149.3	3.2	0.136
D step		na	50%/160 °C/24 h	14.51	na	12,090	105.86	124.6	1.5	0.261
E step		na	50%/170 °C/24 h	13.40	na	141,432	104.92	116.3	0.8	0.313
F step		na	50%/180 °C/24 h	22.32	na	106,140	101.24	112.4	0.8	0.341
G step		na	50%/190 °C/24 h	11.21	na	97,323	98.97	110.8	0.8	0.333
H step		na	50%/190 °C/24 h	0.61	na	4002	105.96	102.8	10.0	0.331
I step		na	Residue digest	0.03	na	554	106.78	157.1	60.0	
Sample 3										
A step	48 hr, 550 °C	na	5%/80 °C/24 h	10.88	na	928	119.50	104.9	6.0	0.129
B step		na	50%/80 °C/24 h	4.51	na	7545	76.27	135.5	2.5	0.096
C step		na	50%/120 °C/24 h	8.26	na	11,907	93.49	127.9	1.5	0.079
D step		na	50%/160 °C/24 h	17.81	na	9179	104.54	121.4	2.0	0.133
E step		na	50%/170 °C/24 h	11.24	na	50,917	105.27	121.0	0.9	0.241
F step		na	50%/180 °C/24 h	21.38	na	116,383	104.41	115.8	0.8	0.316
G step		na	50%/190 °C/24 h	20.27	na	167,387	100.64	112.3	0.8	0.359
H step		na	50%/190 °C/24 h	4.82	na	109,232	102.21	115.3	0.8	0.364
I step		na	Residue digest	0.85	na	14,595	106.88	115.0	3.5	0.380

(continued on next page)

Table 1 (*continued*)

Sample	Anneal	Weight (mg)	PDA conditions	% of total U	U (ppm)	Observed ratio	Calculated ages (Ma)			Calculated ratio
						$^{206}Pb/^{204}Pb$	$^{206}Pb^*/^{238}U$	$^{207}Pb^*/^{206}Pb^*$	Error (2-sigma)	$^{232}Th/^{238}U$
Sample 3										
A step	48 hr, 850 °C	na	5%/80 °C/24 h	8.09	na	603	107.89	99.1	10.0	0.143
B step		na	50%/80 °C/24 h	1.92	na	1491	53.61	127.6	11.0	0.154
C step		na	50%/120 °C/24 h	2.58	na	2548	102.39	132.8	7.0	0.138
D step		na	50%/160 °C/24 h	15.81	na	14,431	105.96	119.2	1.4	0.100
E step		na	50%/170 °C/24 h	15.83	na	49,681	105.77	116.8	0.9	0.162
F step		na	50%/180 °C/24 h	20.04	na	97,655	105.93	115.7	0.8	0.244
G step		na	50%/190 °C/24 h	16.36	na	14,5471	105.22	113.1	0.8	0.317
H step		na	50%/190 °C/24 h	9.54	na	118,998	104.83	112.7	0.8	0.361
I step		na	Residue digest	9.83	na	79,551	105.84	110.8	0.9	0.408
Sample 4										
A step	48 hr, 850 °C	0.55	50%/120 °C/24 h	11.04	5446	2248	79.57	96.5	5.0	0.524
B step		1.79	50%/160 °C/24 h	10.85	1642	17,814	86.91	93.8	1.3	0.418
C step		4.49	50%/170 °C/24 h	18.21	1041	73,830	86.89	90.0	0.8	0.504
D step		1.93	50%/170 °C/24 h	6.77	899	119,650	86.70	89.3	0.8	0.578
E step		4.27	50%/170 °C/24 h	13.25	796	179,150	86.75	89.1	0.8	0.603
F step		3.82	50%/180 °C/24 h	10.63	713	142,516	86.75	89.4	0.8	0.631
G step		3.78	50%/180 °C/24 h	9.73	661	154,945	86.82	89.2	0.8	0.648
H step		3.54	50%/190 °C/48 h	8.63	626	138,092	86.79	90.1	0.8	0.661
I step		4.09	50%/190 °C/48 h	9.43	591	59,992	86.90	89.9	0.9	0.674
J step		0.62	Residue digest	1.46	604	44,692	86.96	91.1	2.1	0.708
Sample 5										
A step	48 hr, 850 °C	0.17	50%/120 °C/24 h	2.20	904	39	96.00	197.5	600.0	0.567
B step		1.01	50%/160 °C/24 h	4.24	298	1599	110.57	127.2	11.0	0.351
C step		2.46	50%/170 °C/24 h	8.40	242	8879	115.07	120.4	2.2	0.375
D step		1.14	50%/170 °C/24 h	3.23	201	17,592	115.49	118.4	1.5	0.411
E step		2.49	50%/170 °C/24 h	7.09	201	26,607	115.57	118.4	1.1	0.420
F step		2.4	50%/180 °C/24 h	6.30	185	28,190	115.61	119.1	1.2	0.437
G step		2.61	50%/180 °C/24 h	6.54	177	30,858	115.62	119.8	1.0	0.450
H step		3.34	50%/180 °C/24 h	7.91	168	38,759	115.63	117.3	0.9	0.462
I step		7.81	50%/190 °C/24 h	18.07	164	34,731	115.38	117.6	1.0	0.479
J step		5.38	50%/190 °C/24 h	11.27	148	64,757	115.49	117.7	0.8	0.502
K step		4.36	50%/190 °C/24 h	9.16	149	26,247	115.55	118.0	1.1	0.517
L step		2.21	50%/190 °C/48 h	4.35	139	11,662	115.45	116.9	2.0	0.531
M step		3.47	50%/190 °C/48 h	6.96	142	21,787	115.51	118.2	1.2	0.542
N step		2.09	Residue digest	4.29	144	42,566	115.59	119.1	1.4	0.567
Sample 6										
A step	48 hr, 1100 °C	0.24	50%/120 °C/12 h	1.71	539	45	135.09	238.1	420.0	2.648
B step		1.91	50%/160 °C/12 h	9.47	377	8101	161.83	173.0	2.5	0.953
C step		3.29	50%/170 °C/12 h	12.70	293	42,717	165.57	168.5	0.9	0.798
D step		5.13	50%/180 °C/12 h	16.80	249	72,054	165.41	167.7	0.8	0.719
E step		3.33	50%/180 °C/12 h	10.40	237	92,494	165.58	168.9	0.8	0.673
F step		6.63	50%/190 °C/12 h	19.59	225	144,970	165.26	167.9	0.8	0.648
G step		4.14	50%/190 °C/12 h	11.35	209	117,213	165.47	167.7	0.8	0.620
H step		3.86	50%/190 °C/12 h	10.07	198	180,050	165.57	167.7	0.8	0.604
I step		1.38	50%/190 °C/12 h	3.46	191	89,348	165.37	169.7	0.8	0.584
J step		1.79	50%/190 °C/12 h	4.44	189	87,094	165.43	167.8	0.8	0.576

Table 1 (*continued*)

Sample	Anneal	Weight (mg)	PDA conditions	% of total U	U (ppm)	Observed ratio	Calculated ages (Ma)			Calculated ratio
						$^{206}Pb/^{204}Pb$	$^{206}Pb^*/^{238}U$	$^{207}Pb^*/^{206}Pb^*$	Error (2-sigma)	$^{232}Th/^{238}U$
Sample 7										
A step	48 hr, 1100 °C	0.41	50%/140 °C/24 h	27.57	2916	444	223.75	403.4	22.0	0.403
B step		0.81	50%/150 °C/24 h	13.39	708	5423	416.78	454.2	3.1	0.250
C step		0.94	50%/150 °C/24 h	8.15	367	22,686	459.05	462.8	1.0	0.268
D step		1.05	50%/150 °C/24 h	6.85	278	46,283	461.16	463.5	0.8	0.288
E step		1.29	50%/155 °C/24 h	7.18	238	73,266	461.35	463.0	0.8	0.301
F step		1.79	50%/160 °C/24 h	8.80	209	122,344	461.85	463.0	0.8	0.313
G step		1.76	50%/160 °C/24 h	7.93	192	161,840	461.53	462.5	0.8	0.324
H step		1.36	50%/160 °C/24 h	6.22	194	137,179	461.70	462.8	0.8	0.333
I step		1.38	50%/165 °C/24 h	6.25	192	150,476	460.74	463.0	0.8	0.340
J step		0.81	50%/165 °C/24 h	3.66	194	84,354	460.91	462.7	0.8	0.346
K step		0.52	50%/170 °C/24 h	2.46	199	56,350	460.13	460.9	0.9	0.350
L step		0.19	50%/175 °C/24 h	1.11	236	26,647	461.14	465.5	2.1	0.354
M step		0.09	50%/190 °C/24 h	0.45	214	4207	459.99	465.8	5.0	0.360

might result from very slight residual leaching effects, minor analytical artifacts (because this sample was run at an early stage in the study prior to use of high-temperature clean-up steps or the 2-vial method), or even very minor inheritance of slightly older zircon that was slightly more soluble than the bulk of the igneous zircon. The result from this un-annealed fraction can be compared to an aliquot of these zircons annealed at 1100 °C prior to PDA (reported in Busby et al., in press) that yields a true plateau age of 110.08 ± 0.11 Ma with MSWD = 0.97. This agreement suggests that, whatever the cause of the apparent slight decline in ages for the sample 1 un-annealed zircon aliquot E–N steps, the total amount of zircon represented by these 10 steps has behaved overall as a closed system, at least to the ca. 0.1% level. The agreement between the annealed and un-annealed age results for this sample also reveals that "simple" PDA (no annealing) can yield valid age results in at least some cases of zircons with low levels of radiation damage for the higher temperature steps (cf. Mattinson, 1994). However, as will be discussed below, this behavior breaks down at higher levels of radiation damage.

Results for sample 2 zircons from a Late Cretaceous pluton from the Sierra Nevada Batholith (kindly supplied by Dr. James Chen; sample KC-13 of Chen and Moore, 1982; $^{206}Pb^*/^{238}U$ age, coarse fraction, reported as 85.1 Ma) are presented in Fig. 2 and Table 1. A large un-annealed fraction was analyzed in 10 PDA steps. The $^{206}Pb^*/^{238}U$ age vs. U released pattern (Fig. 2A) is very similar to that for sample 1,

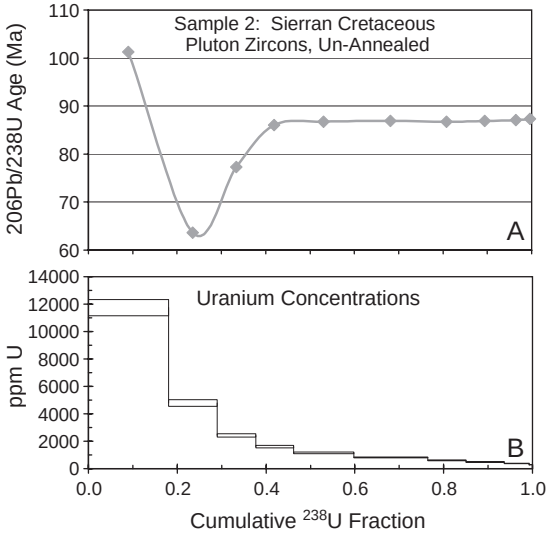

Fig. 2. Multi-step PDA results from sample 2 un-annealed late Cretaceous zircons. (A) The $^{206}Pb^*/^{238}U$ age release pattern is very similar in form to that seen in Fig. 1. However, the strongly disturbed part of the age spectrum extends further in terms of the amount of U released, and the ages for the higher temperature steps show clear excess scatter (see text for discussion). (B) The U concentrations are much higher for this sample than for sample 1, and the differences in isotopic systematics are presumably the result of differences in degree of radiation damage.

discussed above, in terms of the typical "Big Dipper" or "soup ladle" pattern shown by the release spectrum. In this case, however, the early PDA steps remove a much larger proportion of the total U in the sample, despite identical acid strength, temperature, and time progression for these steps compared to sample 1. For sample 2, the A through D steps remove more than 40% of the total U from the zircon sample. This is likely related to the higher U concentrations for sample 2, as shown in Fig. 2B. The "too old" A step has a U concentration of almost 12,000 ppm. The following three "too young" B, C, and D steps have U concentrations of ca. 4800, 2400, and 1600 ppm, respectively. The remaining 6 steps range from ca. 1150 to 300 ppm U, and do not define a plateau, but instead plot with a slight undulation—a slight recumbent "S" shape, barely perceptible in Fig. 2A. An average of these 6 steps yields an age of 86.93 ± 0.25 Ma (2-sigma error; ± 0.2% errors on individual points; MSWD = 7.7). The high MSWD clearly indicates that the 6 higher temperature steps from this un-annealed zircon sample have not behaved as a series of simple closed-system subdomains. Again, comparison with an annealed aliquot of the same zircon sample is useful. An annealed fraction of this sample, discussed later as sample 4, does not show the "S" shape, and yields a high-precision plateau age of 86.83 ± 0.06 Ma (2-sigma error; ± 0.2% errors on individual points; MSWD = 1.05). This strongly indicates that slight but significant leaching effects persisted between the more intense, higher temperature PDA steps in the un-annealed fraction. Nevertheless, the good agreement between the average age for the last 6 steps for the un-annealed sample 2, and plateau age for the annealed sample 4 (86.93 ± 0.25 and 86.83 ± 0.06, respectively) indicates no significant leaching of Pb from the E–J steps by the earlier, lower intensity, clearly disturbed A–D steps. In the absence of data from the annealed aliquot however, it would be difficult to place much reliance on the age from the un-annealed aliquot.

3.3. Effects of progressive annealing

Three aliquots of sample 3, zircons from an Early Cretaceous pluton from the Sierra Nevada Batholith (kindly supplied by Dr. James Chen; sample W-3 of Chen and Moore, 1982; $^{206}Pb^*/^{238}U$ age, coarse fraction, reported as 111.8 Ma), reveal the effects of progressive annealing of radiation damage. These data are a subset of an experiment involving nine aliquots of this zircon that were un-annealed, and annealed for 48 h at 550, 650, 750, 850, 950, 1050, 1150, and 1200 °C, respectively, and each analyzed in nine PDA steps (Mattinson, 2000b). Detailed analysis of the results indicates that this zircon population contains a very small inherited component. Thus, even the strongly annealed split does not display plateau behavior. Also, Zr concentration data are not available for these zircons, so individual steps cannot be discussed in terms of their actual U concentrations. However, the results do provide a good understanding of zircon solubility and leaching effects versus progressive annealing of radiation damage. The un-annealed, 550 °C, and 850 °C results are discussed here, and presented in Fig. 3 and Table 1.

Fig. 3A shows the $^{206}Pb^*/^{238}U$ release spectrum for the sample 3 un-annealed aliquot. It shows the characteristic (and very large) "dipper" pattern for the first few steps. The first three PDA steps remove almost 38% of the total U in the sample. However, the remaining steps fail to define a plateau. Instead they form a recumbent "S" pattern, similar to, but more obvious than that discussed for sample 2 earlier. Clearly, significant leaching effects have penetrated deep into the zircon, and it is not possible to interpret the age of the sample from these data with any confidence.

Fig. 3B shows the spectrum for the sample 3 aliquot annealed for 48 h at 550 °C. In basic form, the release pattern is similar to that for the un-annealed split. However, the "bowl" of the ladle is compressed towards the left side of the diagram, with the first three PDA steps removing 23.6% of the sample U, significantly less than in the un-annealed split. The annealing, even at this relatively low temperature, significantly reduced the solubility of the zircon and reduced the magnitude of the leaching effects. The later PDA steps for the 550 °C split show some flattening of the age pattern compared with the un-annealed split, but still do not form a plateau. Obviously there are still significant leaching effects deep within the zircon grains at this low level of annealing.

Fig. 3C shows the sample 3 split annealed for 48 h at 850 °C. At this level of annealing the bowl of

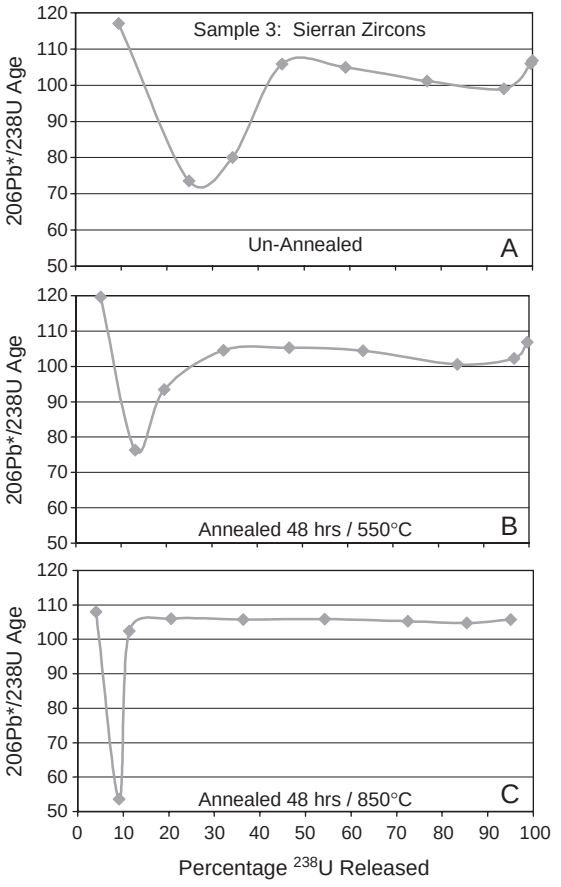

Fig. 3. Age release patterns showing the effects of progressive annealing on three aliquots of sample 3, an Early Cretaceous zircon sample. (A) Un-annealed zircons, showing strong leaching effects, both for the early PDA steps ("big dipper"), and also for the later PDA steps. (B) Zircons annealed for 48 h at 550 °C, showing significant suppression of both solubility and leaching effects, with some compression of the "dipper" towards the left side of the diagram, and some flattening of the pattern of the later PDA steps. (C) Zircons annealed for 48 h at 850 °C, showing further strong suppression of solubility and leaching effects—highly compressed "dipper" pattern and reasonably good age agreement for the higher temperature steps (but not perfect due to minor inheritance).

the ladle is very tightly compressed against the left side of the release diagram, with the first three PDA steps extracting only 12.6% of the total U. The remaining six PDA steps, representing ca. 87.4% of the U, yield ages in reasonably good agreement, but do not define a plateau due to the very minor inheritance discussed above. At this level of annealing, radiation damage has been effectively removed from the moderate to low-U zircon grain interiors. The full range of these experiments (Mattinson, 2000b) plus experiments on other samples (Mattinson, unpublished data) indicate that a useful range of annealing spans ca. 800 °C to 1100 °C for 48 h. In recent work, I have "standardized" the annealing process, using 1000 °C/48 h.

Despite the 48 h/850 °C annealing, the "dipper" pattern for the earliest steps persists, although, as noted above, it is restricted to a very small percentage of the total U. By analogy with samples 1 and 2, these early steps undoubtedly represent very high U, thin, outer zones of the grains with very high levels of radiation damage. The detailed annealing experiments for this sample (Mattinson, 2000b) suggest that such high levels of radiation damage are only removed at annealing temperatures above 950 °C. Also see Nasdala et al. (2001) for an excellent detailed discussion of annealing radiation damage in zircons.

3.4. Full "*CA (chemical abrasion)-TIMS*" *results*

This section discusses samples analyzed by the final "CA-TIMS" method. All were annealed prior to PDA at temperatures of either 850 °C or 1100 °C for 48 h. In addition, the very low intensity early steps have been omitted. Low intensity early steps reveal details of possible residual leaching effects in very thin, very high U+Th rims (possibly too heavily radiation-damaged to be effectively annealed at the lower end of the annealing temperature range, as discussed above). However, they do not influence final age interpretation. For the full CA-TIMS analysis, for reasons of efficiency, an initial more intense step (e.g., 120 °C/24 h/50% HF) replaces the three to four low intensity initial steps discussed in the previous sections. Note, even after annealing, not all zircons respond the same way to a particular set of PDA steps. Radiation damage is clearly the primary control on solubility of un-annealed zircons. However, even after removal of radiation damage by annealing, trace element substitutions cause lattice distortions that can play an important role in determining solubility (e.g. Köppel and Sommerauer, 1974), as discussed in more detail later. Some care and experimentation is useful in determining the optimal PDA temperature progression.

Results for sample 4 are shown in Fig. 4 and Table 1. Sample 4 is an aliquot of the KC-13 (Chen and Moore, 1982; $^{206}Pb^*/^{238}U$ age, coarse fraction, reported as 85.1 Ma) zircons discussed earlier as Sample 2, which was not annealed prior to PDA. In contrast, Sample 4 was annealed for 48 h at 850 °C. Prior to annealing it was also moderately air-abraded (Krogh, 1982) as a test of the air abrasion process. A comparison of the U-release patterns for samples 2 and 4 (Figs. 2B and 4B, respectively), indicates much lower U concentrations for the early steps for Sample 4. Thus, as expected, air abrasion removed a significant amount of high-U rim material from the zircon. However, the $^{206}Pb^*/^{238}U$ release spectrum (Fig. 4A), reveals that slight discordance remains after air abrasion. The initial step (24 h/120 °C), released about 11% of the total U, with an average U concentration of ca. 5400 ppm and a $^{206}Pb^*/^{238}U$ age of ca. 79.6 Ma. The true "closed-system" age of the zircons is given by the plateau of the remaining nine steps (89% of the total U, ca. 1640 to 600 ppm for steps B–J, respectively) as 86.83 ± 0.06 Ma (2-sigma). The "bulk

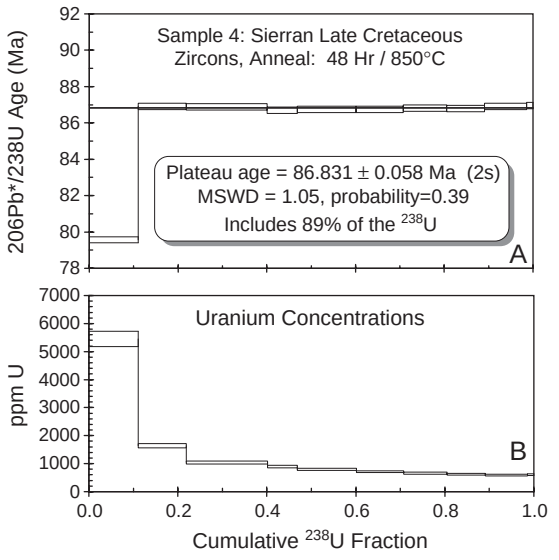

Fig. 4. CA-TIMS results for sample 4, an aliquot of the sample 2 zircons, but in this case moderately abraded, then annealed for 48 h at 850 °C. (A) $^{206}Pb^*/^{238}U$ age release spectrum defines a plateau, plotted using the Ar/Ar step heating program from Isoplot (Ludwig, 2000b), that yields a precise and accurate age. Heights of the boxes show 2-sigma errors of 0.2% on the ages. (B) U concentration results—note both similarities and contrasts to Fig. 2B—see text for discussion.

$^{206}Pb^*/^{238}U$ age" or "total ^{238}U age" of the air-abraded zircons, obtained by recombining all the age steps, weighted by fraction of U released in each step, is 86.03 Ma, indicating that after moderate air abrasion, the zircons were still ca. 0.9% discordant. More extreme air abrasion certainly would have reduced the level of discordance still further, by removing more of the outer, high-U zircon material. However, it is important to note that <1% levels of Pb loss are difficult to detect in samples of this age range by conventional U–Pb analysis. Classical definitions of concordance (e.g. agreement of $^{206}Pb^*/^{238}U$ and $^{207}Pb^*/^{206}Pb^*$ ages within errors) tend to break down at this level; ages that can be considered "concordant within errors" might actually be "discordant within errors". Detailed population statistics of large numbers of abraded single grain ages (e.g., Mundil et al., 2001) can reveal excess scatter in the ages, indicative of small variable amounts of Pb loss (or inheritance). However, it is extremely difficult to demonstrate complete removal of Pb loss effects in conventional, air abrasion analyses, whereas this is clearly achieved and clearly demonstrated by the CA-TIMS method with its combined annealing, multi-step PDA, and plateau data analysis approach.

As mentioned earlier, for the full CA-TIMS procedure, the initial PDA step (in this case 120 °C/24 h/50% HF) replaces a series of more delicate steps used for un-annealed zircons and progressive annealing experiments. It seems quite likely that a compressed "dipper" pattern (cf. Fig. 3C) would also be revealed for Sample 4 if these more delicate and detailed early PDA steps had been applied. Such a pattern would suggest that radiation damage in the very outermost, very high U+Th zones of the zircon were not fully annealed at 48 h/850 °C. However, the high-quality age plateau from Sample 4 strongly indicates that, for the zircon domains represented by the plateau steps, radiation damage has been successfully annealed. This could represent total annealing of radiation damage, or at least annealing of enough of the radiation damage so that leaching effects are eliminated. Despite this compelling evidence for elimination of radiation damage, and presumably elimination of solubility differences related to radiation damage, Fig. 4B reveals that the PDA steps still show a simple dissolution progression from higher U to lower U zircon domains. This is a crucial point, and clearly indicates

that, even after annealing of radiation damage, zircon solubility still varies systematically with U concentration. Magmatic zircons commonly show strong core to rim U+Th zonation. Thus, simple physical access (rim first, core last) could explain the order of dissolution. However, dissolution along microcracks, etc., commonly provides access for acid to penetrate grain interiors (e.g., Mattinson et al., 1996, Fig. 5). Thus, a view of dissolution control via pure physical rim to core access is likely incomplete.

It has long been known that there is a strong positive correlation between U+Th concentrations and the concentrations of other trace elements (e.g., P, Y, Ca, REE). Furthermore, high concentrations of U, Th, and other trace elements cause distortions of the zircon lattice, rendering it less stable, and more susceptible to weathering or any other chemical attack (e.g., Köppel and Sommerauer, 1974). Again, given the typical magmatic zircon pattern of core to rim increase in U and other trace elements, this residual solubility contrast, based on trace element-induced lattice distortion, would strongly reinforce a rim to core dissolution progression based on simple physical access. This means that CA-TIMS steps progressively sample compositionally distinct zircon domains, ca. from rim to core: early steps typically remove high-U rim material ± some high U zones from deeper within the grains (the latter inaccessible to air abrasion); later steps sample lower-U material, progressively deeper into the cores of the grains. Thus each CA-TIMS step represents a geochemically unique sub-sample of zircon, rather than a blurred average of the entire zircon mass.

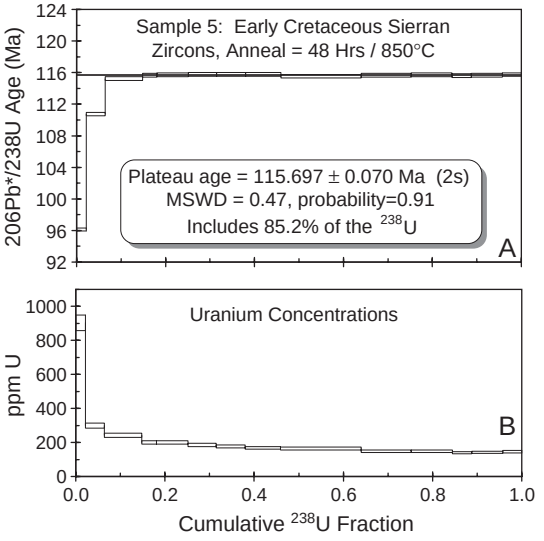

Fig. 5. CA-TIMS results for sample 5, a relatively low-U, Early Cretaceous zircon sample annealed for 48 h at 850 °C. (A) $^{206}Pb^*/^{238}U$ age release spectrum—note evidence for moderate to very slight Pb loss for the first three CA-TIMS steps, and the small amount of U (15%) released in these steps. The remaining 11 PDA steps define a plateau that yields a very precise and accurate age (2-sigma errors for the individual steps=0.2%). (B) The plot of U concentrations reveals a minor amount of moderate-U rim material removed in the first step, followed by low-U material making up the bulk of the zircon.

Results from zircons from an Early Cretaceous Sierran pluton, Sample 5 (kindly provided by Dr. James Chen; sample W10 of Chen and Moore, 1982; $^{206}Pb^*/^{238}U$ age reported as 114.2 Ma) are shown in Fig. 5 and Table 1. These zircons were annealed at 850 °C for 48 h, analyzed in 14 steps, and are very well behaved. The first three of the 14 PDA steps show moderate to very slight Pb loss, yielding $^{206}Pb^*/^{238}U$ ages of ca. 96 Ma, 110.7 Ma, and 115.2 Ma, and U concentrations of ca. 900 ppm, 300 ppm, and 240 ppm for steps A–C, respectively (Fig. 5A,B). The remaining 11 PDA steps have U concentrations ranging from ca. 200 ppm to 140 ppm for steps D–N, respectively, and evidently represent perfect closed-system behavior. These steps yield a precise plateau age of 115.697 ± 0.070 Ma. For well-behaved plutonic samples in this age range, the plateau errors are in the range of the life spans of magma chambers (e.g., Coleman et al., 2004), allowing resolution of very fine-scale chronologies of pluton emplacement over short geologic time scales.

Results from zircons from a Late Jurassic ophiolite plagiogranite, sample 6 (San Simeon remnant, California Coast Range ophiolite, Mattinson, 1987; $^{206}Pb^*/^{238}U$ age reported as 165.43 ± 0.34 Ma) are shown in Fig. 6 and Table 1. These zircons were annealed at 1100 °C for 48 h, analyzed in 10 steps, and also yield very well-behaved CA-TIMS systematics (Fig. 6A). The A and B steps show moderate to slight Pb loss, with ages of ca. 135 and 162, and U concentrations of ca. 540 ppm and 380 ppm, respectively (Fig. 6B). Together, these first two steps only remove ca. 11% of the total U in the sample. The remaining eight steps, ranging from ca. 290 ppm to 190 ppm U, yield a closed-system $^{206}Pb^*/^{238}U$ plateau age of 165.46 ± 0.12 Ma. With rare exceptions, ophio-

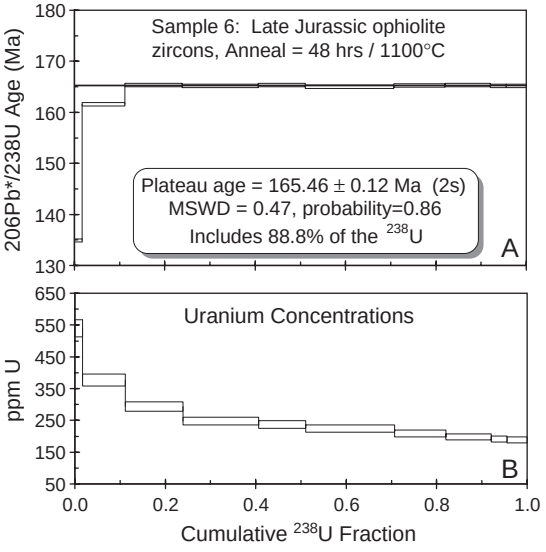

Fig. 6. CA-TIMS results for sample 6, a late Jurassic ophiolite zircon sample annealed for 48 h at 1100 °C. (A) the $^{206}Pb^*/^{238}U$ age release spectrum is very similar to Fig. 5A in terms of moderate to slight Pb loss from the earliest two CA-TIMS steps, and the plateau formed by the remaining eight steps, and yielding a precise and accurate age (2-sigma errors for the individual steps=0.2%). (B) The plot of U concentrations is quite similar to that shown in Fig. 5B, with a small moderate-U first step, followed by a series of lower-U steps.

lite plagiogranite zircons lack inheritance, and are thus excellent candidates for high accuracy $^{206}Pb^*/^{238}U$ CA-TIMS dating. In the case of large ophiolite exposures perpendicular to a paleo-ridge, the high precision of the CA-TIMS method holds promise for direct determination of spreading rates.

Results for zircons from an early Paleozoic pluton from the Klamath Mountains, sample 7 (=81P-210 from Wallin et al., 1988; upper intercept age reported as 469 ± 21 Ma) are shown in Fig. 7 and Table 1. The zircons were annealed a 1100 °C for 48 h. These zircons combine strong U zonation (Fig. 7B) with a much older age than the samples discussed previously. As a result, the outer rims of the zircons contain a large proportion of the total U in the sample, were heavily radiation damaged, and lost large amounts of Pb via natural discordance processes. Thus, this is an especially rigorous test of the CA-TIMS method. The A step removed a very high percentage of the total U in the sample – almost 28% – and is very strongly discordant, having lost more than 50% of its Pb and yielding a $^{206}Pb^*/^{238}U$ age of only ca. 224 Ma. The combination of a U concentration of 2916 ppm plus the ca. 461 Ma age of this sample makes this the most heavily radiation damaged (assuming minimal natural annealing of radiation damage) and most discordant step in this study. The B step removes another ca. 13% of the total U, and is moderately discordant, yielding

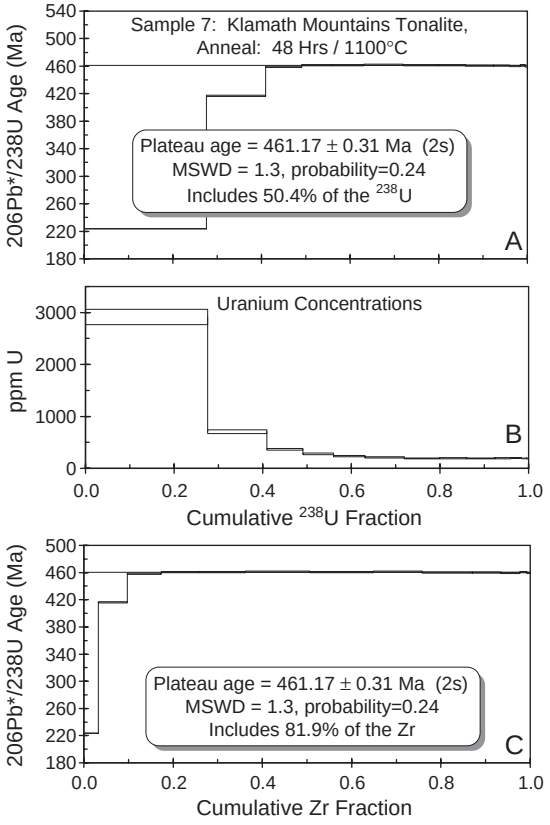

Fig. 7. CA-TIMS results for sample 7, an Early Paleozoic zircon sample annealed for 48 h at 1100 °C. (A) The $^{206}Pb^*/^{238}U$ age release spectrum shows a very large and very strongly discordant first CA-TIMS step, a large and moderately discordant second CA-TIMS step, followed by a very slightly discordant third step, then a plateau (2-sigma errors for the individual steps=0.2%). (B) The U concentrations shed considerable light on the age spectrum. These zircons have thin, high-U rims that dominate the U balance of the early CA-TIMS steps, are heavily radiation damaged, and have lost major amounts of Pb. The interiors of the zircon grains, however, have relatively low U concentrations are have remained closed to Pb loss. (C) The same $^{206}Pb^*/^{238}U$ age release spectrum is plotted here against the actual amount of zircon removed by each step, rather than the amount of U released. This reveals how selective the CA-TIMS method is in removing zircon domains that have lost Pb. Ca. perfect closed system behavior has been achieved after removal of only ca. 18% of the actual mass of the zircons.

an age of 417 Ma. As shown in Fig. 7B, the U concentrations show the typical strong decrease from early to late PDA steps—the U concentration for the B step is much lower than that for the A step, at 708 ppm. The C step is still lower in U, at 367 ppm, and shows only very slight Pb loss, yielding an age of 459 Ma. Compared to the plateau age of 461.17 Ma (below), the C step shows an apparent Pb loss of just under 0.5%. As shown in Fig. 7A and B, the remaining 10 steps range in U concentration from ca. 280 to 190 ppm, show excellent closed-system behavior, and define a $^{206}Pb^*/^{238}U$ plateau with an age of 461.17 ± 0.31 Ma. This sample demonstrates the power of the CA-TIMS method to extract highly precise and accurate ages, even from strongly disturbed samples. The same data set is plotted in Fig. 7C, but using the actual amount of zircon digested rather than U released on the abscissa. This highlights the exceptional selectivity of the CA-TIMS method, which targets the high-U, high-trace element (usually outer) zones of the zircon grains with the early partial dissolution steps. In this case, perfect closed-system (plateau) behavior is reached after removing almost 50% of the U from the zircons (Fig. 7A), but this represents removal of only ca. 18 % of the mass of the zircons (Fig. 7C).

This paper has focused on describing and documenting the potential of the new CA-TIMS method for dating zircon. The specific examples, excepting sample 3, have all been zircon samples that do not contain any detectable older inherited component, so that the complete elimination of any leaching effects could be clearly demonstrated. For such samples, the $^{206}Pb^*{}^{238}U$ age plateau is clearly the most precise and accurate measure of the crystallization age of the zircons, and also the most robust demonstration of the power of the CA-TIMS method. To avoid a manuscript of excessive length, detailed presentations and discussions of $^{207}Pb^*/^{206}Pb^*$ ages, and a range of other geochemical data that can be obtained via the CA-TIMS method have been omitted from the earlier discussion, and will be presented in detail elsewhere. However, for completeness, two additional sets of data are presented here for sample 7: $^{207}Pb^*/^{206}Pb^*$ data, and $^{232}Th/^{238}U$ data.

$^{207}Pb^*/^{206}Pb^*$ results for sample 7 are presented in Fig. 8A and Table 1. Typically, early PDA steps of the CA-TIMS method remove most or all of the initial Pb from a zircon sample. Evidently the initial Pb is

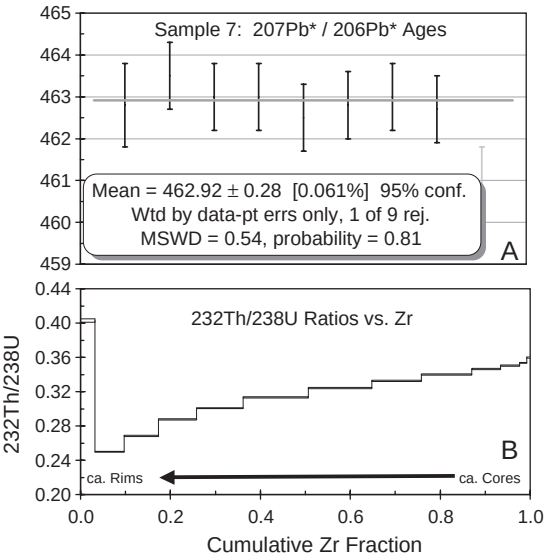

Fig. 8. $^{207}Pb^*/^{206}Pb^*$ ages and Th/U ratios for sample 7 zircons. (A) All $^{207}Pb^*/^{206}Pb^*$ ages from the plateau steps that yield 2-sigma errors of 1 Ma or less. Excluding one slightly low result, eight steps are in excellent agreement using the Isoplot (Ludwig, 2000b) weighted average (see text for discussion). (B) $^{232}Th/^{238}U$ ratios (calculated from $^{208}Pb^*/^{206}Pb^*$ ratios) reveal a moderate decline in Th/U in the magma for most of the history of zircon crystallization from zircon cores (right side of graph) to rims (left side of graph). The trend of Th/U ratios is sharply reversed during crystallization of the outer rims of the zircons. See text for discussion.

associated with the outer, high-U + Th + trace element rims of most zircons, and with tiny inclusions of other minerals that are relatively soluble compared to zircon. Later PDA steps yield $^{206}Pb/^{204}Pb$ ratios that are very high, subject only to the limitations of the amount of sample Pb* relative to the Pb blank. Thus, high quality $^{207}Pb^*/^{206}Pb^*$ ages and plateau results can be obtained, subject to the limitations (e.g., decay constant uncertainties, intermediate daughter disequilibrium, etc.) discussed earlier. The results for sample 7 are fairly typical, with the earliest steps yielding poor precision due to relatively high common Pb content, followed by later steps with $^{206}Pb/^{204}Pb$ observed ratios mostly in the tens of thousands to hundreds of thousands. For these PDA steps, the largest source of uncertainty in the $^{207}Pb^*/^{206}Pb^*$ ratio is the uncertainty in the mass fractionation correction (not necessarily true of very small samples where mass spectrometer counting statistics might predominate).

$^{207}Pb^*/^{206}Pb^*$ ages for the nine steps with 2-sigma errors of 1 Ma or less are shown in Fig. 8A. One slightly low age was rejected. The remaining eight ages give an error-weighted mean of 462.92 ± 0.28 Ma 2-sigma, MSWD = 0.54. The $^{207}Pb^*/^{206}Pb^*$ ages have been adjusted for an 80% 230Th exclusion at the time crystallization (a relatively small correction of ca. 0.4 Ma for zircons in this age range). The $^{207}Pb^*/^{206}Pb^*$ ages still are slightly older than the $^{206}Pb^*/^{238}U$ plateau age by just under 2 Ma. However, this is well within the 2-sigma errors in the U decay constants (e.g., Jaffey et al., 1971; Mattinson, 1987; Ludwig, 2000a). More detailed analysis of the U decay constants is beyond the scope of this paper, and will be presented elsewhere. The key point here is that the $^{207}Pb^*/^{206}Pb^*$ ages are in excellent agreement, within analytical and decay constant uncertainties, with the $^{206}Pb^*/^{238}U$ plateau age. This is a further strong indication that the plateau steps have sampled zircon that has behaved as a perfectly closed system, and confirms the robustness of the $^{206}Pb^*/^{238}U$ plateau approach.

$^{232}Th/^{238}U$ results are presented in Fig. 8B and Table 1. These data (and other trace element data from CA-TIMS steps) provide insight into the evolution of magma during the crystallization history of the zircon population, and also provide a further understanding of the CA-TIMS dissolution process. $^{232}Th/^{238}U$ ratios for zircons can be obtained directly by isotope dilution of Th as well as U, or indirectly from $^{208}Pb^*/^{206}Pb^*$ ratios. The latter approach was used in this study. First, it is necessary to briefly examine the role of zircon in recording and controlling the $^{232}Th/^{238}U$ ratios in the magma from which it has crystallized. It is well known that zircon has high partition coefficients for both U and Th, but in detail, preferentially incorporates U, relative to Th (for a recent review, see Parrish and Noble, 2003). Thus, ideally, zircon provides direct data about the Th/U ratio of the magma. However, this is a "moving target" during the crystallization history of the magma. If zircons were the dominant control of the U and Th balance in the magma, Th/U ratios would be driven up in the residual magma as more and more zircon crystallized. This increase in Th/U would then be recorded in the growing zircons themselves, from core to rim. If, however, other U- and Th-bearing minerals are important, even predominant, in determining the U and Th mass balance, zircon will still record these effects, but no longer control them. Minerals such as apatite, titanite, and especially monazite can also be important in the overall Th/U evolution in a crystallizing magma. Monazite is an extreme case of a mineral that very strongly incorporates Th relative to U. Thus, crystallization of monazite, or any other U- and Th-bearing mineral with Th > U, will tend to drive down the Th/U ratio in the magma.

The Th/U ratios for sample 7 (Fig. 8B) in general show a consistent decline from the right-hand side of the diagram (last CA-TIMS steps = ca. early crystallized zircon cores) to the left-hand side (early CA-TIMS steps = ca. late crystallized zircon rims). The first step, in contrast, indicates an increase in Th/U during the very last stage of zircon crystallization. This overall pattern suggests that the Th/U ratio of the evolving magma has in fact been dominated by high Th/U minerals, rather than by zircon, driving the Th/U ratio of the magma down during crystallization. However, at the very end of crystallization, the Th/U ratio increased sharply. This is suggestive of a sealing up of "permeability" in the rock during the final stages of magmatic crystallization. In other words, zircon grains are no longer in "communication" via diffusion with other U- and Th-bearing minerals, but are isolated in tiny sealed pockets of residual magma (cf. Dempster et al., 2003 who discuss a similar effect for trace elements in apatite). Zircon's strong preference for U over Th then drives up the Th/U during this very last phase of magmatic crystallization. Alternatively, the high T/U for the first CA-TIMS step could reflect tiny grains of a high Th/U mineral adhering to or included in the outermost rim of the zircons. This seems much less likely, given the very large amount of both U and Th in the A step, however.

The strong core to rim zoning of U and Th in general, as discussed earlier for most of the samples in this study, is a very common characteristic of magmatically crystallized zircons, and is also relevant to interpreting CA-TIMS steps. The typical pattern of relatively low-U + Th cores and high-U + Th rims for zircon grains is of course related to the fact that zircon and other U + Th-bearing minerals tend to be trace minerals. In terms of mass balance, the U and Th concentrations in the residual magma is driven up by the crystallization of major minerals that contain

ca. no U or Th (e.g., quartz, feldspars) as opposed to being driven down by the crystallization of the zircon and other high U+Th minerals.

Both the systematic patterns of Th/U ratios and U concentrations from early to late CA-TIMS steps demonstrate that the steps in general progressively sample from outer zircon rim material to deep zircon core material. The systematic Th/U patterns are further strong evidence that the plateau steps also represent a series of distinct sub-samples of zircon grains, as suggested earlier on the basis of U concentrations. The plateau steps are not some fortuitous exactly equal mixture of components of two or more different ages, or an even more fortuitous mixture of just the right proportions of variably discordant zircon plus concordant zircon such that each plateau step has exactly the same age.

4. Summary and conclusions

Multi-step chemical abrasion (CA-TIMS) provides a powerful new method for high-resolution U–Pb analysis of zircons. Pre-PDA annealing evidently entirely eliminates radiation-damage-mediated leaching effects from lightly to moderately radiation-damaged zircon domains, permitting very high-accuracy $^{206}Pb^*/^{238}U$ plateau ages to be determined from zircons that lack inheritance. Of particular importance is the ability to remove all parts of zircons that have been affected by Pb loss in early PDA steps, and then to recognize the undisturbed parts of the zircons via statistical agreement of the remaining (plateau) steps. The plateau ages typically show precisions of better than 0.1%. Given that the ^{238}U decay constant is very accurately determined (Jaffey et al., 1971), and that corrections for initial deficit of ^{230}Th can be made with reasonable confidence for all but very young samples, $^{206}Pb^*/^{238}U$ plateau age accuracies can also be at the sub-0.1% level, excluding only the (non-trivial) problem of high-accuracy isotopic tracer calibration.

A crucial feature of the CA-TIMS method lies in the selectivity of the dissolution steps. The progression of dissolution steps can be easily understood in terms of a combination of physical accessibility plus solubility-inducing lattice distortions caused by high U+Th+correlated trace-element concentrations (e.g., Köppel and Sommerauer, 1974). Since the zones with the highest U+Th+correlated trace-element concentrations are commonly also the outermost zones, due to normal magmatic zoning, they are easily accessed by the earliest steps. These same zones are also the most susceptible to natural Pb loss. Thus, their removal by the early CA-TIMS steps leaves a low U+Th, closed-system residue. However, as noted by Mattinson (1994), the dissolution progression is not entirely a simple rim to core progression. Instead, microcracks, etc., provide access for the HF to mine out high-U+Th zones deep within zircon grains. These same microcracks might have provided access for corrosive natural fluids to remove Pb from the deep interiors of grains. The ability of the CA-TIMS method to mine out domains that reside deep within grains, but still have lost Pb is a significant advantage over the widely used and otherwise highly successful air abrasion method (Krogh, 1982), which is limited to removal of only the outermost layers. For the same reasons, CA-TIMS can isolate and analyze closed-system domains within zircon grains that would be considered "low-quality" by conventional grain selection techniques.

The step-to-step variations in U+Th+correlated trace elements, and Th/U ratios for CA-TIMS steps also demonstrate that each CA-TIMS step is geochemically distinct, as opposed to a series of steps simply being more or less identical averages of a wide range of zircon zones. This is particularly strong evidence for the validity of the plateau ages by the CA-TIMS method.

High-precision $^{207}Pb^*/^{206}Pb^*$ plateau ages are also possible. However, especially for Late Paleozoic and younger zircons, the accuracy of such ages is more difficult to assess. First, even very small errors in decay constants propagate into highly magnified errors in calculated $^{207}Pb^*/^{206}Pb^*$ ages (e.g., Mattinson, 1987; Ludwig, 2000a). Next, for Mesozoic and especially Tertiary samples, uncertainties in ^{230}Th corrections are significant. Particularly in plutonic rocks in which zircon is saturated only for part of the crystallization history, and in which a range of other minerals contribute to the Th/U mass balance in the magma, corrections based on comparing the bulk zircon Th/U ratio with the bulk rock Th/U ratio are overly simplistic. Such corrections probably are reasonably accurate in the case of volcanic rocks with a

modest percentage of phenocrysts, however. Finally, ^{231}Pa corrections (in the ^{235}U→^{207}Pb* decay chain) are fraught with major uncertainty. There is no long-lived isotope of Pa available to allow direct comparison of the Pa/U ratio between zircon and bulk rock. Incorporation of large amounts of excess Pa (in turn generating excesses of ^{207}Pb*) in zircon has been convincingly demonstrated by Mortensen et al. (1992, 1997) and Anczkiewicz et al. (2001). Anczkiewicz et al. (2001) point out that Pa can have either a +4 or +5 valence, depending on oxidation conditions, and that Pa in the +5 state could be highly compatible in zircons, thus explaining the excesses. The ^{231}Pa (=^{207}Pb*) excesses reported in these studies are very large, and such excesses could even have significant effects on the calculated ^{207}Pb*/^{206}Pb* ages of Proterozoic and Archean rocks. Pa excesses very much smaller than those reported by Mortensen et al. (1997) and Anczkiewicz et al. (2001), if common in zircons, would limit the accuracy of high-precision ^{207}Pb*/^{206}Pb* ages, especially in Paleozoic and younger rocks. Thus, for "young" samples, the classical definition of U–Pb "concordance" becomes less useful in many cases at the highest levels of precision. Instead, for zircons lacking inheritance, a high-quality ^{206}Pb*/^{238}U plateau is excellent evidence for concordance, and the plateau age affords the greatest accuracy for magmatic crystallization ages.

Multi-grain zircon fractions containing older inherited components do not yield plateau ages. In fact, once effects of Pb loss have been removed by early CA-TIMS steps, an age progression from step to step is an extremely sensitive detector of inheritance, with each step representing a different mixture of the various (commonly multiple) zircon components (Mattinson, unpublished data). In such cases, single grain methods are essential for obtaining accurate crystallization ages (e.g., Bowring and Erwin, 1998; Mundil et al., 2001). CA-TIMS is also adaptable to single grain zircon dating, as explored below.

Much of the power of the CA-TIMS method lies in the plateau approach. The ability to remove zircon domains that have been affected by Pb loss, and then define an age plateau of several steps, allows for a high level of confidence in the accuracy of the age determination. However, the multi-step plateau approach requires a zircon sample large enough to contain sufficient Pb* for each step to have adequate precision, sample/blank ratio, etc. This becomes problematic for analysis of most single zircon grains. Moreover, one of the strengths of single grain analysis lies in the analysis of large numbers of single grains, and the use of careful statistical analysis to reject any grains with inheritance or Pb loss (e.g., Mundil et al., 2001). In cases where it is desirable to analyze a large number of grains rather than do detailed analysis of a few grains, or where very small grain size actually would preclude multiple plateau steps, a modified CA-TIMS approach can be applied. For example, a series of tests can determine, for a particular suite of zircons, how intense a PDA step is required to strip off the parts of zircon grains that have experienced Pb loss. Individual grains can then be subjected to a single "clean-up" step of at least this intensity, followed by total digestion of the remaining zircon—i.e. a simple two-step procedure. The requirements are simply that all discordant parts of the grain are removed by the "clean-up" step (ideally with a large degree of "overkill"), while still leaving a residue large enough to analyze with the desired precision. Highly successful application of this approach has already been demonstrated by Mundil et al. (2004). Mundil (Chemical Geology reviewer's comment) also notes that: "...the application of the technique does not require a significant increase in cost or time...".

Alternatively, a multi-grain population could be subjected to a series of "early" CA-TIMS steps, with full isotopic analysis after each step. Once the isotopic systematics of the population clearly indicated elimination of all Pb loss, the desired number of individual grains could be selected from the residue for single-grain analysis. A further alternative that combines the efficiency of the two-step analysis with some of the power of the plateau approach would be to subject each of several grains to a different clean-up step intensity. Agreement of a number of residues from different clean-up temperatures would increase confidence that the ages represented perfect closed-system zircon domains.

Finally, the CA-TIMS method has the potential to make a significant contribution in the area of both characterizing and preparing zircon standards for inter-laboratory TIMS U–Pb calibrations, and for ion probe and laser ablation-ICP-MS analysis. First, CA-TIMS analysis can reveal the presence or

absence, at very low levels, of zircon complexities such as inheritance and/or Pb loss in standards that are in use, or are being considered for use. Next, the ability of CA-TIMS to remove domains that are discordant due to Pb loss could be taken advantage of in preparing standards for use. Based on the results of complete CA-TIMS evaluation of zircons, a series of steps adequate for removing all discordant parts of zircon grains would produce a residue of concordant zircon material for use as standards. For ion probe and LA-ICP-MS, just the annealing stage of the CA-TIMS process might result in more reproducible results for standards and unknown zircon samples alike, by removing possible sputtering or ablation artifacts related to differing degrees of natural radiation damage in un-annealed zircons (e.g. Romer, 2003).

Acknowledgements

This paper is dedicated to Dr. George Tilton and Dr. Tom Krogh, two giants in the development of U–Pb zircon geochronology, and also my mentors, colleagues, and friends. Some of the zircons for this study have been provided by Dr. James Chen, who generously gave me full access to his extensive collection of zircons from Sierra Nevada plutons. Helpful and constructive reviews by Brad Hacker, Chris Mattinson, Bill McClelland, Roland Mundil, George Tilton, and an anonymous reviewer significantly improved the manuscript. Funding for various aspects of the study have been provided by NSF (EAR-9418560, and EAR-0073602). **[PD]**

References

Anczkiewicz, R., Oberli, F., Burg, J.P., Villa, I.M., Günther, D., Meier, M., 2001. Timing and normal faulting along the Indus Suture in Pakistan Himalaya and a case of major $^{231}Pa/^{235}U$ initial disequilibrium in zircon. Earth Planet. Sci. Lett. 191, 101–114.

Bowring, S.A., Erwin, D.H., 1998. A new look at evolutionary rates in deep time: uniting paleontology and high-precision geochronology. GSA Today 8 (9), 1–8.

Busby, C., Fackler-Adams, B., Mattinson, J.M., DeOreo, S., in press. View of an intact oceanic arc, from surficial to mesozonal levels: Cretaceous Alisitos arc, Baja California. J. Volcanol. Geotherm. Res.

Cherniak, D.J., Watson, E.B., 2000. Pb diffusion in zircon. Chem. Geol. 172, 5–24.

Chen, J.H., Moore, J.G., 1982. Uranium–lead isotopic ages from the Sierra Nevada Batholith, California. J. Geophys. Res. 87, 4761–4784.

Chen, F., Siebel, W., Satir, M., 2002. Zircon U–Pb and Pb-isotope fractionation during stepwise HF acid leaching and geochronological implications. Chem. Geol. 191, 155–164.

Coleman, D.S., Gray, W., Glazner, A.F., 2004. Rethinking the emplacement and evolution of zoned plutons: geochronological evidence for incremental assembly of the Tuolumne intrusive suite, California. Geology 32 (5), 433–436.

Corfu, F., 2000. Extraction of Pb with too-old ages during stepwise dissolution experiments on Archean zircon. Lithos 53, 279–291.

Davis, D.W., Krogh, T.E., 2000. Preferential dissolution of ^{234}U and radiogenic Pb from (alpha)-recoil-damaged lattice sites in zircon: implications for thermal histories and Pb isotopic fractionation in the near-surface environment. Chem. Geol. 172, 41–58.

Dempster, T.J., Jolivet, M., Tubrett, M.N., Braithwaite, C.J.R., 2003. Magmatic zoning in apatite: a monitor of porosity and permeability change in granites. Contrib. Mineral. Petrol. 145, 568–577.

Jaffey, A.H., Flynn, K.F., Glendenin, L.E., Bently, W.C., Essling, A.M., 1971. Precision measurement of the half-lives and specific activities of U235 and U238. Phys. Rev., Ser. C 4, 1889–1906.

Köppel, V., Sommerauer, J., 1974. Trace elements and the behavior of the U–Pb system in inherited and newly formed zircons. Contrib. Mineral. Petrol. 43, 71–82.

Krogh, T.E., 1973. A low contamination method for the hydrothermal decomposition of zircon and extraction of U and Pb for isotopic age determinations. Geochim. Cosmochim. Acta 37, 485–494.

Krogh, T.E., 1982. Improved accuracy of U–Pb zircon ages by the creation of more concordant systems using an air abrasion technique. Geochim. Cosmochim. Acta 46, 637–649.

Krogh, T.E., Davis, G.L., 1974. Alteration in zircons with discordant U–Pb ages. Carnegie Inst. Yearbook 73, 560–567.

Krogh, T.E., Davis, G.L., 1975. Alteration in zircons and differential dissolution of altered and metamict zircon. Carnegie Inst. Yearbook 74, 619–623.

Lee, J.K.W., Williams, I.S., Ellis, D.J., 1997. Pb, U, and Th diffusion in natural zircon. Nature 390, 159–162.

Ludwig, K.R., 2000a. Decay constant errors in U–Pb concordia-intercept ages. Chem. Geol. 166, 315–318.

Ludwig, K.R., 2000b. Isoplot/Ex 2.45, a geochronological toolkit for Microsoft Excel: Berkeley Geochronology Center.

Mattinson, J.M., 1987. U–Pb ages of zircons: a basic examination of error propagation. Chem. Geol., Isot. Geosci. Sect. 66, 151–162.

Mattinson, J.M., 1994. A study of complex discordance in zircons using step-wise dissolution techniques. Contrib. Mineral. Petrol. 116, 117–129.

Mattinson, J.M., 1997. Analysis of zircon by multi-step partial dissolutions: the good, the bad, and the ugly. GAC/MAC Ottawa '97 Abst. Vol., A98.

Mattinson, J.M., 2000a. Low-temperature U–Pb discordance mechanisms in zircons: the role of radiation damage and fluids. Fall Meeting Suppl., Abstract V21D-35, Eos Trans, AGU, vol. 81 (48).

Mattinson, J.M., 2000b. U–Pb zircon analysis by "chemical abrasion": combined high-temperature annealing and partial dissolution analysis. Suppl. Eos, Trans.-Am. Geophys. Union 8 (19), S27 (GS32A-02).

Mattinson, J.M., 2003. CA (chemical abrasion)-TIMS: high-resolution U–Pb zircon geochronology combining high-temperature annealing of radiation damage and multi-step partial dissolution analysis. Fall Meeting Suppl., Abstract V22E-06, Eos, Trans, AGU, vol. 84 (46).

Mattinson, J.M., Graubard, C.M., Parkinson, D.L., McClelland, W.C., 1996. U–Pb reverse discordance in zircons: the role of fine-scale oscillatory zoning and sub-micron transport of Pb. In: Basu, J.M., Hart (Eds.), Earth Processes: Reading the Isotopic Code, Geophysical Monograph, vol. 95. American Geophysical Union, pp. 355–370.

McClelland, W.C., Mattinson, J.M., 1996. Resolving high precision U–Pb ages from Tertiary plutons with complex zircon systematics. Geochim. Cosmochim. Acta 60 (20), 3955–3965.

Mortensen, J.K., Roddick, J.C., Parrish, R.R., 1992. Evidence for high levels of unsupported radiogenic 207 Pb in zircon from a granitic pegmatite: implications for interpretation of discordant U–Pb data. Abstracts, 1992 Spring Meeting, AGU, Supplement to EOS, pp. 370.

Mortensen, J.K., Williams, I.S., Compston, W., 1997. Ion microprobe and cathodoluminescence investigations of unsupported 207 Pb in zircon. GAC/MAC Annual Meeting Abstract Volume, Ottawa, ON, 1997, pp. A105.

Mundil, R., Metcalfe, I., Ludwig, K.R., Renne, P.R., Oberli, F., Nicoll, R.S., 2001. Timing of the Permian–Triassic biotic crisis: implications from new zircon U/Pb age data (and their limitations). Earth Planet. Sci. Lett. 187, 131–145.

Mundil, R., Ludwig, K.R., Metcalfe, I., Renne, P.R., 2004. Age and timing of the Permian mass extinctions: U/Pb dating of closed-system zircons. Science 305, 1760–1763.

Nasdala, L., Wenzel, M., Vavra, G., Irmer, G., Wenzel, T., Kober, B., 2001. Metamictization of natural zircon: accumulation versus thermal annealing of radioactivity-induced damage. Contrib. Mineral. Petrol. 141, 25–144.

Nasdala, L., Wenzel, M., Vavra, G., Irmer, G., Wenzel, T., Kober, B., 2002. Metamictization of natural zircon: accumulation versus thermal annealing of radioactivity-induced damage (correction). Contrib. Mineral. Petrol. 143, 767–768.

Parrish, R.R., Noble, S.R., 2003. Zircon U–Th–Pb geochronology by isotope dilution–thermal ionization mass spectrometry (ID-TIMS). In: Hanchar, J.M., Hoskin, P.W.O. (Eds.), Zircon, Reviews in Mineralogy and Geochemistry, 53, pp. 183–213.

Romer, R.L., 2003. Alpha-recoil in U–Pb geochronology: effective sample size matters. Contrib. Mineral. Petrol. 145, 481–491.

Silver, L.T., Deutsch, S., 1963. Uranium–lead isotopic variations in zircons: a case study. J. Geol. 71, 721–758.

Tilton, G.R., 1956. Interpretation of lead–age discrepancies by acid-washing experiments. Trans.-Am. Geophys. Union 37, 224–230.

Tilton, G.R., Patterson, C.C., Brown, H., Inghram, M., Hayden, R., Hess, D., Larsen Jr., E., 1955. Isotopic composition and distribution of lead, uranium, and thorium in a Precambrian granite. Geol. Soc. Amer. Bull. 66, 1131–1148.

Todt, W.A., Büsch, W., 1981. U–Pb investigations on zircons from pre-Variscan gneisses: I. A study from the Schwartzwald, West Germany. Geochim. Cosmochim. Acta 45, 1789–1801.

Wallin, E.T., Mattinson, J.M., Potter, A.W., 1988. Early Paleozoic magmatic events in the eastern Klamath Mountains, northern California. Geology 16, 144–148.

Wetherill, G.W., 1956. Discordant uranium–lead ages. Trans.-Am. Geophys. Union 37, 320–326.